Diffusion in a Fluid Membrane with a Flexible Cortical Cytoskeleton

Thorsten Auth[†§*] and Nir S. Gov[‡]

[†]Department of Materials and Interfaces, and [‡]Department of Chemical Physics, The Weizmann Institute of Science, Rehovot, Israel; and [§]Institute for Solid State Research, Research Centre Jülich, Jülich, Germany

ABSTRACT   We calculate the influence of a flexible network of long-chain proteins, which is anchored to a fluid membrane, on protein diffusion in this membrane. This is a model for the cortical cytoskeleton and the lipid bilayer of the red blood cell, which we apply to predict the influence of the cytoskeleton on the diffusion coefficient of a mobile band 3 protein. Using the pressure field that the cytoskeleton exerts on the membrane, from the steric repulsion between the diffusing protein and the cytoskeletal filaments, we define a potential landscape for the diffusion within the bilayer. We study the changes to the diffusion coefficient on removal of one type of anchor proteins, e.g., in several hemolytic anemias, as well as for isotropic and anisotropic stretching of the cytoskeleton. We predict an overall increase of the diffusion for a smaller number of anchor proteins and increased diffusion for anisotropic stretching in the direction of the stretch, because of the decrease in the spatial frequency as well as in the height of the potential barriers.

INTRODUCTION

Diffusion within the fluid membrane plays an important role for cellular processes, because the cell communicates with its surrounding via its lipid bilayer. For example, diffusion of activated receptor molecules leads to signal amplification (1) and diffusion of adhesion molecules to the contact area is important for cell adhesion (2). Diffusion in the membrane has to be small enough to allow proper localization of extracellular signals (3). Further discussion of the functional role of diffusion within the cell membrane can be found in Saxton (4). To increase our understanding of the interaction of the cell with its environment, it is important to understand the diffusion of lipids and proteins in the plasma membrane.

The diffusion coefficient of lipids in an intact red blood cell (RBC), is of order $D \approx 1 \ \mu m^2 \, s^{-1}$, whereas the diffusion coefficient of a typical membrane protein, such as the mobile component of band 3 (that is a common protein in RBC membranes), is two orders of magnitude smaller (band 3 has a free, mobile fraction and a cytoskeleton-bound fraction, which is immobile) (5). Saffmann and Delbrück found that the diffusion is slower for an increased size of the diffusing molecule (6), but according to their theory the size dependence is only logarithmic and not able to explain the large difference between the diffusion coefficients of a membrane protein and a lipid. The inverse dependence of the diffusion coefficient on the protein diameter found in Gambin et al. (7) will not suffice. Furthermore, the diffusion coefficient of band 3 in artificial dimyristoylphosphatidylcholine membranes was found to be three orders of magnitude larger than in intact cells (5).

The cytoskeleton, which is in close proximity to the membrane, acts as a strong regulator of the diffusion within the cellular membrane. The evidence for this role comes from various experiments. Experiments show that the spectrin cytoskeleton of the RBC slows down translational diffusion (8–13), and proteins diffuse considerably faster on membrane blebs of muscle cells that are free from the cytoskeleton compared with the intact cell membrane containing the cytoskeleton (14). Using single molecule tracking techniques, small compartments have been found for the diffusion in the cell membrane (15), that may be explained by the cytoskeletal network below the bilayer. Further general discussion about the cytoskeletal influence on the diffusion in the lipid bilayer is found in the review articles (4,5,16–18).

In principle, several interaction mechanisms between the cytoskeleton and the molecules in the lipid bilayer are possible. In mechanism 1, proximity of the cytoskeleton to the bilayer alters the local viscosity and therefore the local diffusion coefficient. The diffusing molecules stick to the cytoskeletal filaments in mechanism 2, or the molecules of the cytoskeleton act as physical barriers for diffusion in mechanism 3. Mechanism 1 has not attracted much interest up to now and the magnitude of the effect is still unclear (19–21). We neglect the hydrodynamic interaction of the diffusing particle with the bulk fluid, by which the cytoskeleton could indirectly alter the diffusion coefficient. Mechanism 2 proposes that sticking of membrane proteins or lipids to the cytoskeleton (22–25) hinders diffusion by confinement of the diffusing molecules to attractive cytoskeletal elements (26). Sticking has been found to explain the slower lateral diffusion of lipids in supported bilayers compared with the diffusion in free bilayers (27,28). However, in the RBC membrane, mobile proteins such as band 3 seem to be squeezed out of areas with a dense underlying cytoskeletal network and to be enriched in areas with a dilated network

(29), which does not seem to be compatible with a sticky cytoskeleton. The fact that the fast rotational diffusion of free band 3 in RBCs is not affected by the presence or absence of the cytoskeleton (30), whereas the translational diffusion is strongly hindered by an intact cytoskeleton, has been interpreted in Sheetz (9) as an indication for mechanism 3; the cytoskeleton acts as a physical barrier for protein diffusion and forms corrals. A similar reasoning is found in Corbett et al. (31). The importance of such barriers for the patchiness of lipid membranes is discussed in Gheber and Edidin (32). Compartments that have been found with single particle tracking experiments support the barrier model (15,17,18,33,34).

Many models are based on the corral hypothesis (9,35,36). In Saxton (37), a percolation analysis is used for a spectrin network with defects, and transient bonds that can be passed with a given probability (e.g., caused by conformational fluctuations of the spectrin) are discussed. Saxton (38) investigates the influence of transient bonds and the dependence of the diffusion and the elastic properties on the state of the network. Such a transient bond network could also explain why the barrier-free pathlength that is found by dragging proteins with tweezers in the cell membrane is larger than the cytoskeletal mesh size (39). In addition, the models in Saxton's work (37,38) already incorporate possible dissociation of spectrin tetramers into dimers or detachment of spectrin molecules from the actin/band 4.1 complex. Attachment and detachment of spectrin molecules may be driven by ATP, as suggested by Sheetz and Casaly (10) and Gov and Safran (40), or induced by stretching of the bonds (41). To justify dynamic corral models (38,42,43), conformational fluctuations of the flexible spectrin polymer away from the plane of the bilayer (21,38) or of the bilayer itself (44–46) are sufficient to allow diffusing molecules to leave a corral.

This study focuses on the diffusion in the membrane of cells that have a cortical, two-dimensional cytoskeleton, which is composed of flexible long-chain proteins (47). A prominent example of such cells are RBCs (48), where the long-chain proteins are spectrin tetramers, but a similar cortical cytoskeleton is found on the plasma membrane of other mammalian cells (4), and spectrin has been identified in neurons (49) and on membranes of intracellular organelles (50). Our model presents a general computation of the effects of an anchored network of flexible molecules on the diffusion in the fluid membrane to which this network is attached. This model should therefore be relevant to many biological and synthetic systems, some of which are listed above. We apply our model to the special case of band 3 diffusion in the RBC membrane, because this is a well studied system with available experimental data (8,51–53).

We introduce what we believe is a new model that quantifies effects of excluded-volume (steric hindrance) on the diffusion inside the bilayer membrane, due to an anchored network of flexible long-chain proteins. The long-chain proteins exert a pressure field on the (flat) fluid membrane that repels diffusing molecules (the pressure field locally bends the membrane, but the pressure-induced bending of a flat RBC membrane has been predicted to be only a few nanometers in height (47); our model does not take into account the effects of membrane fluctuation (54) and membrane curvature (55,56) on the diffusion). The cytoskeletal filaments therefore act as soft potential barriers; this approach allows the calculation of the escape probability of the protein from the corral uniquely (57). According to the ''wall theorem'', the polymer pressure is proportional to the probability that the polymer chain touches the membrane (58). It is straightforward to define the potential barriers for the in-plane diffusion, because they are simply proportional to the cytoskeletal pressure on the membrane, $p(\boldsymbol{\rho})$ where $\boldsymbol{\rho} = (x,y)$. The barrier height felt by the diffusing molecule depends on its interaction volume, v, that protrudes into the cytoplasm and interacts with the cytoskeletal filament, $V(\boldsymbol{\rho}) = vp(\boldsymbol{\rho})$. This interaction volume depends on the shape of the diffusing molecule and has to be determined from experimental data. Our model allows us to calculate the effects of lack of proteins that anchor the cytoskeleton to the bilayer and of cytoskeletal stretching on the in-plane diffusion (the effect of stretching a cortical, RBC-like cytoskeleton on in-plane diffusion has been discussed, but not calculated in Boal (59)).

For simplicity, we consider only networks with fixed connectivity, and do not account for processes of filament detachments and network reorganization (10,40). The real cytoskeleton of the RBC contains numerous defects with various kinetics that effectively increase the area of the individual corral. The main properties of the RBC cytoskeleton network not described in our calculations include: i), the spectrin filaments form tetramers that can break into disconnected dimers, especially when the cell is stretched (60); ii), the end points of the filaments can detach from the anchor proteins due to shear and metabolic processes (40); and iii), certain domains in the spectrin molecules can unfold when they are highly stretched (61). These effects can be added in future refinements of our model, by allowing the processes of filament detachment, contour length changes (unfolding), and rearrangements of the connectivity resulting in network remodeling. Before these complex processes are modeled, it is useful to first describe a more simple system, as we do in this study.

Using a random walker and Metropolis Monte Carlo, we determine the effective diffusion coefficients of proteins that are affected by the pressure field of the cytoskeleton (62). We find that the diffusion depends on the density of anchor points between the cytoskeletal network and the membrane, and on the degree of stretching of this network. Most notably, for anisotropic stretching (keeping the network area constant), we find that the effective diffusion increases in the direction of the stretch and decreases in the perpendicular direction.

THEORY

We first describe the calculation of the pressure field due to the cytoskeletal network as a superposition of the pressure fields of the individual filaments. The pressure field of each filament is obtained by a Greens function calculation (47), combined with a simple model that takes into account the finite contour length of each spectrin tetramer ($L = 200$ nm). We assume that the attachment points of the filaments to the membrane are stationary, which is well justified by simulations that show that the chains move much more wildly than the anchor points (59). Our use of a stationary pressure field for the cytoskeleton interaction with the diffusing molecules is justified due to the following estimation: spectrin radius of gyration, $R_g \approx 10$ nm, viscosity of cytoplasm, $\eta_{cytoplasm} \approx 3\eta_{water} \approx 3 \ 10^{-3}$ Pa s, Zimm time $\tau = \eta R_g^3/(k_B T) \approx 7.5\ \mu s$, $D = 0.25$ nm^2 s^{-1} (8), $\sqrt{\langle r^2 \rangle}|_{t=\tau} = 1.4$ nm. The Zimm time of the spectrin molecule in which the filament changes conformation is $\tau \simeq 8\mu s$, and during this time a typical membrane protein diffuses 1 nm, which is small compared with the overall width of the potential barrier of the filament (≈ 10 nm) (Fig. 1).

The pressure field of a linear, flexible polymer that is attached to a hard wall with both ends is determined by the coordinates of its anchors, $\boldsymbol{\rho}_1 = (x_1, y_1)$ and $\boldsymbol{\rho}_2 = (x_2, y_2)$, and by its bulk radius of gyration, R_g. The pressure (47)

$$
\begin{aligned}
p(\boldsymbol{\rho}, R_g) &= \frac{k_B T}{4\pi R_g^2} e^{(\boldsymbol{\rho}_1 - \boldsymbol{\rho}_2)^2/(4R_g^2)} e^{-(|\boldsymbol{\rho}_1 - \boldsymbol{\rho}| + |\boldsymbol{\rho}_2 - \boldsymbol{\rho}|)^2/(4R_g^2)} \\
&\quad \frac{|\boldsymbol{\rho}_1 - \boldsymbol{\rho}| + |\boldsymbol{\rho}_2 - \boldsymbol{\rho}|}{|\boldsymbol{\rho}_1 - \boldsymbol{\rho}|^3 |\boldsymbol{\rho}_2 - \boldsymbol{\rho}|^3} [|\boldsymbol{\rho}_1 - \boldsymbol{\rho}||\boldsymbol{\rho}_2 - \boldsymbol{\rho}| \\
&\quad \left((|\boldsymbol{\rho}_1 - \boldsymbol{\rho}| + |\boldsymbol{\rho}_2 - \boldsymbol{\rho}|)^2 - 6R_g^2 \right) \\
&\quad + 2R_g^2 (|\boldsymbol{\rho}_1 - \boldsymbol{\rho}| + |\boldsymbol{\rho}_2 - \boldsymbol{\rho}|)^2],
\end{aligned}
\tag{1}
$$

diverges close to the anchor points and decreases exponentially for large distances from the anchors, $|\boldsymbol{\rho} \gg \boldsymbol{\rho}_i|$ $(i = 1, 2)$.

The derivation of Eq. 1 is based on the diffusion equation to calculate the polymer conformation (47). This implies that neither self-avoidance effects within the polymer chain nor the Kuhn length (that is twice the persistence length) and the contour length of the polymer are taken into account (the path of a diffusing particle can bend on an arbitrarily small scale, thus the Kuhn length of such a Gaussian chain vanishes whereas its contour length diverges; it can be seen from the exponential decay of the polymer pressure for large distances from the anchor points that there is no finite contour length in the model, otherwise the pressure would drop to zero beyond some distance from the anchor points). The effect of self-avoidance may be considered to be small if the correct radius of gyration is used (58,63) and the flexible chain approach can be used as long as the Kuhn length is small enough. The contour length of the chain, L, is crucial for this work, especially when we stretch the chains up to large fractions of L.

In Winkler (64) and Winkler and Reineker (65), a Gaussian polymer model is combined with the condition of a finite
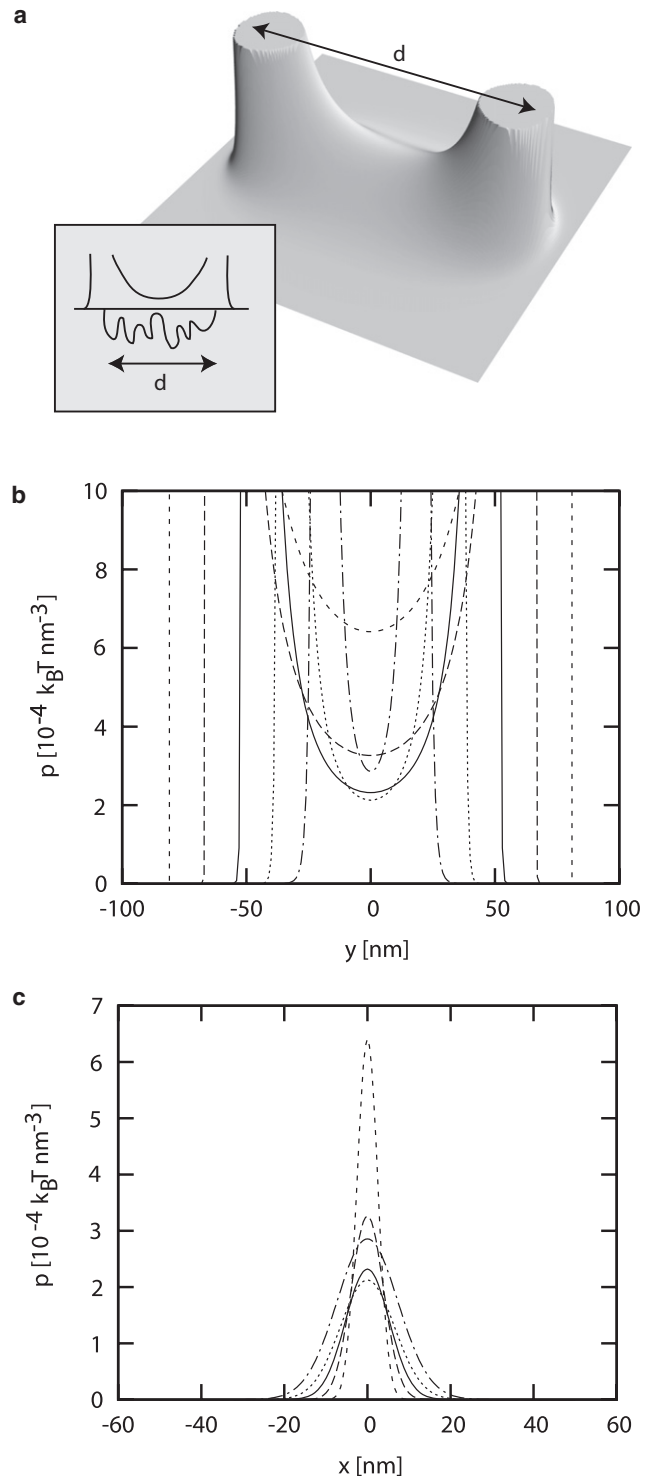
FIGURE 1 Entropic pressure that a flexible cytoskeletal protein exerts on the bilayer membrane. (*a*) Pressure field as obtained from Eq. 1. Pressure profiles parallel (*b*) and perpendicular (*c*) to the connection between the anchor points. Data for a polymer with radius of gyration, $R_g = 14$ nm, and Kuhn length, $\ell = 5.5$ nm, (contour length $L = 214$ nm) for different distances, d, between the anchor points: $d = 40$ nm (*dashed-dotted*), $d = 70$ nm (*dotted*), $d = 100$ nm (*solid*), $d = 130$ nm (*long dashes*), $d = 160$ nm (*short dashes*).

contour length. For flexible as well as semi-flexible chains, force-extension relations, and end-to-end distribution functions have been calculated and the analytic theory describes experimental and simulation data very well (64). We use a simple argument to illustrate the basic mechanism of a finite contour length to obtain an expression analogous to Eq. 1: we subtract from the contour length, $L = 6R_{g,0}^2/\ell$ (where $\ell = L/N$ is the Kuhn length of the polymer, N the number of repeat units in the chain, and $R_{g,0}$ the radius of gyration of the free chain), the anchor distance, d, because this length of the chain is needed to connect the anchor points and is therefore not available for conformation fluctuations. To calculate the pressure field of the stretched chain, we simply replace R_g in Eq. 1 for the free chain by the new, effective R_g, which we obtain using the effective Kuhn length, $\ell' = (L - d)/N$: $R_g^2 = \ell'^2 N/6 = (\ell/6)(L - d)^2/L$.

In Fig. 1, we plot the pressure profile of a single polymer bond: a), along a line that connects both anchor points, and b), in the perpendicular direction along the midline between the anchor points. We use values for the free radius of gyration, $R_{g,0} = 14$ nm, and the Kuhn length, $\ell = 5.5$ nm (i.e., contour length $L \approx 214$ nm), that are close to those known for the RBC spectrin tetramers. The distance between the anchors is varied between $d = 40$ nm and $d = 160$ nm, whereas the observed values for the relaxed RBC are ~60–100 nm (66). For a small distance between the anchor points, the pressure in the middle between the anchors increases with decreasing anchor distance because of the high-pressure regions around the

anchor points (Fig. 1 a). For a large distance of the anchors, the pressure in the middle between the anchor points increases with the anchor distance, because the stretching brings the polymer closer to the membrane along the straight line between the anchors (and depletes it everywhere else). In the limit of the completely stretched out polymer bond, we expect an infinite pressure (hard-core barrier) along the straight line connecting the anchor points (because the polymer lies on the membrane) and zero pressure everywhere else. There is therefore a separation, $d \approx 100$ nm, where the pressure at the midpoint between the anchors is minimal.

Fig. 2 shows a superposition of the single-filament pressure fields for an idealized arrangement of spectrin bonds on a hexagonal lattice, as in the RBC cytoskeleton. The pressure fields for cytoskeletal networks of various deformations are shown; nondeformed and uniaxially stretched with a factor 1.5 and accordingly compressed in the perpendicular direction, such that the total area is conserved. Note that the spatial frequency of cytoskeletal bonds decreases in the direction of the stretching, independent of the orientation of the network. Furthermore, from the isolines of equal pressure, it can be seen that the pressure along stretched bonds increases.

Simulation

To simulate the diffusion process in the lipid bilayer, we use a random walk in two dimensions. The step length is $a = 1$ nm, which is the typical size of the lipid molecules.
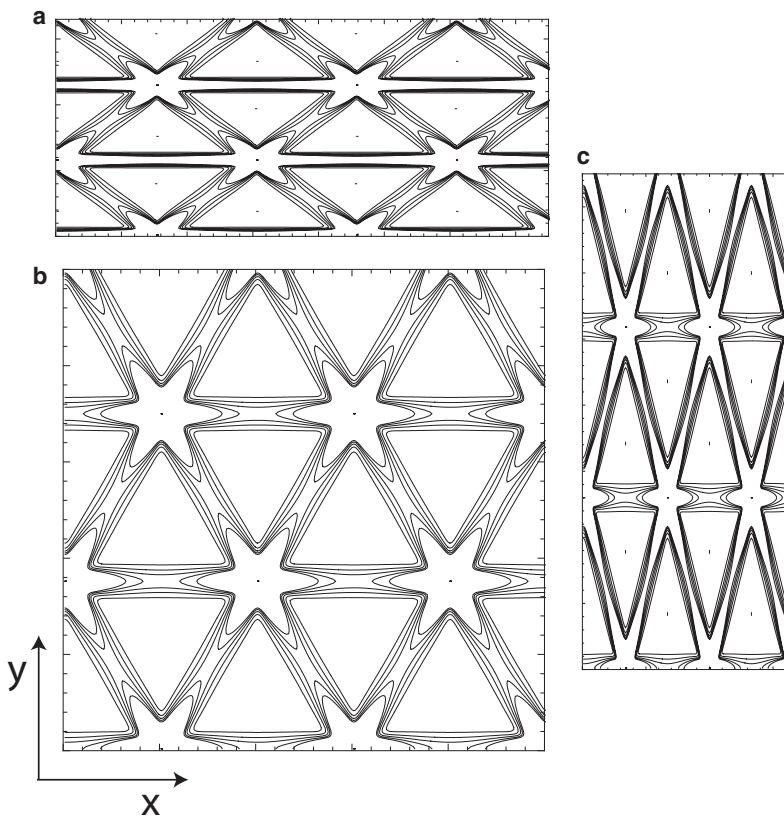

FIGURE 2 Red blood cell cytoskeletal pressure field for polymers with $R_g = 14$ nm, $\ell = 5.5$ nm, and an unstretched bond length of $d = 100$ nm. (a) Cytoskeleton stretched with factor 1.5 in x direction and compressed accordingly in y direction such that the total area is conserved. (b) Unstretched cytoskeleton. (c) Cytoskeleton stretched with factor 1.5 in y direction.
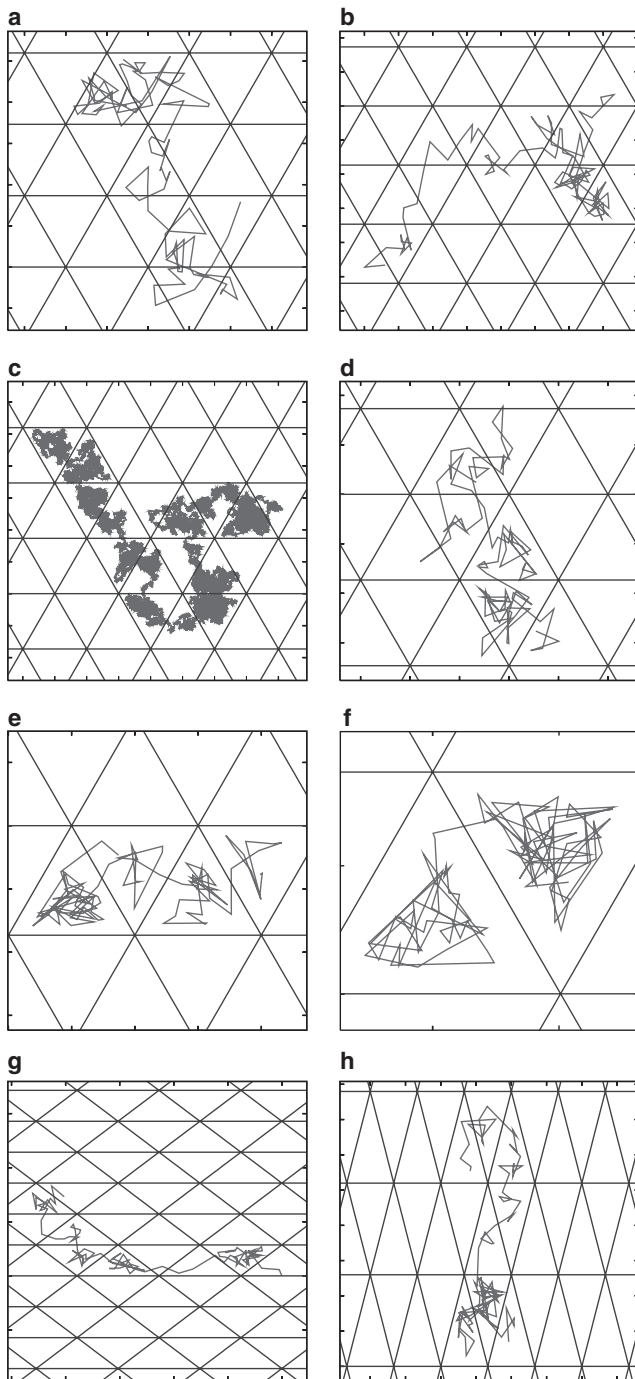
FIGURE 3 Simulation snapshots of a particle diffusing within the lipid bilayer under influence of the potential landscape that is defined by the cytoskeletal pressure. Cytoskeletal bonds have an unstretched bond length $d = 100$ nm and are sketched using straight lines; for better visibility the coarse-grained path of the diffusing particle connects the particle positions only every 1000 simulation steps (except subfigure (c)). The length of the overall path is 100,000 simulation steps each. All plots show a square region of the cell membrane, the tick distance is 50 nm. Snapshots are plotted for the unstretched cytoskeleton and several effective interaction volumes of the diffusing particle, v, as well as for two stretched cytoskeletons: (a) unstretched, $v = 2000$ nm^3; (b) unstretched, $v = 6000$ nm^3; (c) unstretched, $v = 6000$ nm^3, position shown every simulation step; (d) unstretched, $v = 10,000$ nm^3; (e) unstretched, $v = 20,000$ nm^3; (f) un-

The diffusion coefficient for the free membrane is adjusted to values that have been measured in experiments without cytoskeleton. The influence of the cytoskeleton is taken into account by the potential landscape that is determined by the pressure field of the cytoskeleton multiplied with the effective interaction volume, v, for the protein under consideration. Metropolis Monte Carlo (67) is used for the random walker: diffusion steps toward a location with lower energy are always accepted whereas diffusion steps toward a location with higher energy are rejected with the probability, $P(\Delta E) = 1 - \exp[-\Delta E/(k_B T)]$. The energy difference is obtained from the pressure difference between the (possible) future and the present location, $\Delta E = v\Delta p$. The effective interaction volume is obtained from electron microscopy data for spectrin and the diffusing protein or phenomenologically from measurements of the effective diffusion coefficient.

Fig. 3 shows simulation snapshots for diffusion in a potential landscape that corresponds to the RBC cytoskeleton with the spectrin molecules anchored only at the vertices of the network to the lipid bilayer membrane (RBC without ankyrin). In Fig. 3, a–f, the path of a diffusing particle is shown for an unstretched cytoskeleton with bond length, $d = 100$ nm, and for different values of the interaction volume.

In all snapshots, the diffusion of the particle has been observed for equal times, thus on average the length of the observed path should be longer for smaller values of the effective interaction volume. This does not have to hold for each single snapshot, as seen for the snapshots with $v = 2000$ nm^3 and $v = 6000$ nm^3. However, with increasing interaction volume the diffusing molecule is observed to spend longer times in the cytoskeleton-free regions (corrals) than at the location of the bonds, which leads to a hopping motion. For high enough interaction volume, $v = 40,000$ nm^3, the particle is not observed to leave the single compartment during the simulation time.

For the stretched cytoskeletons in Fig. 3, g and h, the particle diffuses preferably in the direction of the stretch, as seen in the snapshots. For the hexagonal lattice, the two situations of stretching in x direction as well as in y direction are qualitatively different, but the effect on the diffusion coefficient parallel and perpendicular to the stretch is similar, as shown in the next section.

We extract the diffusion coefficients, D, by fitting a straight line to the mean-square protein displacement (MSD) for distances that are much larger than a single compartment, $\langle r^2 \rangle = 4Dt$ (Fig. 4). At long times, normal diffusion is observed, but with a smaller diffusion coefficient compared with diffusion without the cytoskeleton. Anomalous diffusion is found for the crossover between the long-time, slow

stretched, $v = 30,000$ nm^3; (g) stretched with factor 1.5 in x direction, $v = 6000$ nm^3; (h) stretched with factor 1.5 in y direction, $v = 6000$ nm^3. The trajectories in (g) and (h) are inconclusive whether the diffusion is enhanced parallel or perpendicular to the direction of the stretch, because these trajectories are too short. Quantitative data for the anisotropy of the diffusion over long times is plotted in Fig. 6 b.
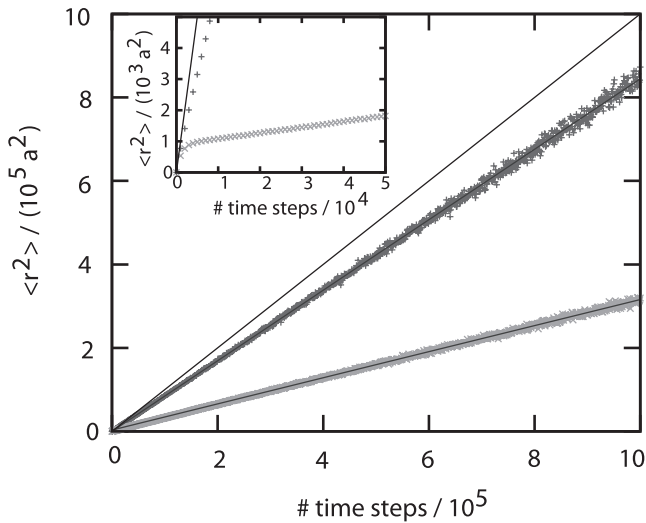
FIGURE 4 Mean-square displacement of a diffusing particle in the membrane. The solid lines give (from top to bottom) the free diffusion without cytoskeleton with diffusion coefficient D_0, the fits to the simulated diffusion in the potential landscapes with interaction coefficients $v = 2000 \text{ nm}^3$ and $v = 10{,}000 \text{ nm}^3$ (the simulation data is indicated by dark "+" for a cytoskeleton without ankyrin anchors and light "x" for a cytoskeleton with ankyrin anchors respectively; see Fig. 5). The diffusion for lengths that are large compared with the mesh size of the cytoskeleton is normal, but with reduced diffusion coefficients, $D_{v=2000\text{nm}^3}=0.84(1)D_0$ and $D_{v=10{,}000\text{nm}^3}=0.31(1)D_0$. The inset shows the mean-square displacement of proteins with $v = 6000 \text{ nm}^3$ for short times. The solid line gives the free diffusion.

diffusion and the short-time, fast diffusion within a single corral. In the inset of Fig. 4, we plot the early times of the MSD, both for a system with extra midpoint anchor complexes (ankyrin) and without, using $v = 6000 \text{ nm}^3$ (Fig. 5). We find a sharp crossover for the system with the ankyrin anchor complexes, as observed in Tomishige et al. (52), whereas we get a smooth crossover when these extra anchor complexes are missing. The sharp crossover can be also found without anchor complexes for larger values of v.

The value of the crossover MSD in our calculations is $\approx 1000 \text{ nm}^2$, which is ~5 times smaller than observed in the experiment (52). A possible reason for this discrepancy could be that the perfect hexagonal network in our calculation constrains the diffusion into corrals that are too small, whereas in the real RBC the network contains many defects that effectively increase the area of the individual corral. In Tomishige
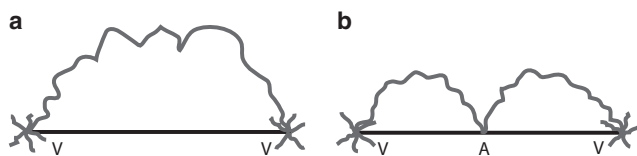

FIGURE 5 (a) RBC without ankyrin: spectrin tetramer that is only anchored to the lipid bilayer at the vertices of the cytoskeletal network (V), where it is also connected to five other tetramers as indicated in the figure. (b) RBC with ankyrin: spectrin tetramer that is anchored at the vertices (V) as well as in the middle of each filament via the ankyrin anchor complex (A).

et al. (52), the corral size is determined from the crossover value; in our simulations, the corral size for the diffusion is given by construction of the cytoskeletal network and does not need to be determined from the crossover value. For a distance of 100 nm between the cytoskeletal vertices as for our unstretched cytoskeleton, the corral size in the simulations is $\approx 4300 \text{ nm}^2$, which is only about a factor two smaller than estimated in Tomishige et al. (52). The hop rate is thus twice as large, $\approx 6 \text{ s}^{-1}$. Due to the large repulsion from the anchor points, the particle does not diffuse over the entire corral (Fig. 3), giving rise to the smaller effective crossover value. From Figs. 6 a and 7 a, we note that a relatively small change in the interaction volume parameter v corresponds to a large change in the diffusion coefficient (and the hop rate). Because the interaction volume is not well known, it can be used as the fit parameter. However, the value for the interaction volume that is determined from the fits is of the same order of magnitude as the value obtained from structural studies.

RESULTS

We present results for cytoskeletal filaments that are anchored to the lipid bilayer at their ends (that models the RBC without the band-3-ankyrin anchor complex) as well as for filaments that are anchored also at their midpoints (RBC with ankyrin) (Fig. 5).

In a healthy RBC, the cytoskeleton is attached to the lipid bilayer at the vertices of the network as well as at the midpoint of the spectrin filament. The latter linkage, which involves the proteins band 3 and ankyrin, can be damaged in disease (68). The presence or absence of this additional anchor changes the fluctuation properties of each spectrin bond: i), it modifies the elastic properties of the spectrin as an entropic spring (41); and ii), it changes the polymer-membrane interaction. The additional anchor brings the spectrin filament closer to the bilayer, which increases the pressure that the conformational fluctuations exert on the lipid bilayer.

RBC without ankyrin

In Fig. 6 a, long-time diffusion coefficients for proteins that diffuse in the potential landscape of the unstretched cytoskeleton are shown as a function of the interaction volume, v. For the unstretched hexagonal network (Fig. 2 b), the diffusion along the x and y directions is found to be equal within the simulation errors for all values of the interaction volume. In the semi-logarithmic plot, the diffusion is non-Arrhenian for small barrier heights: the decrease of the effective diffusion coefficient with increasing barrier height (i.e., with increasing v) is stronger than the exponential decrease that is expected from the Arrhenius law for the transition rate between two minima in the potential landscape, separated by a potential barrier with height E_b

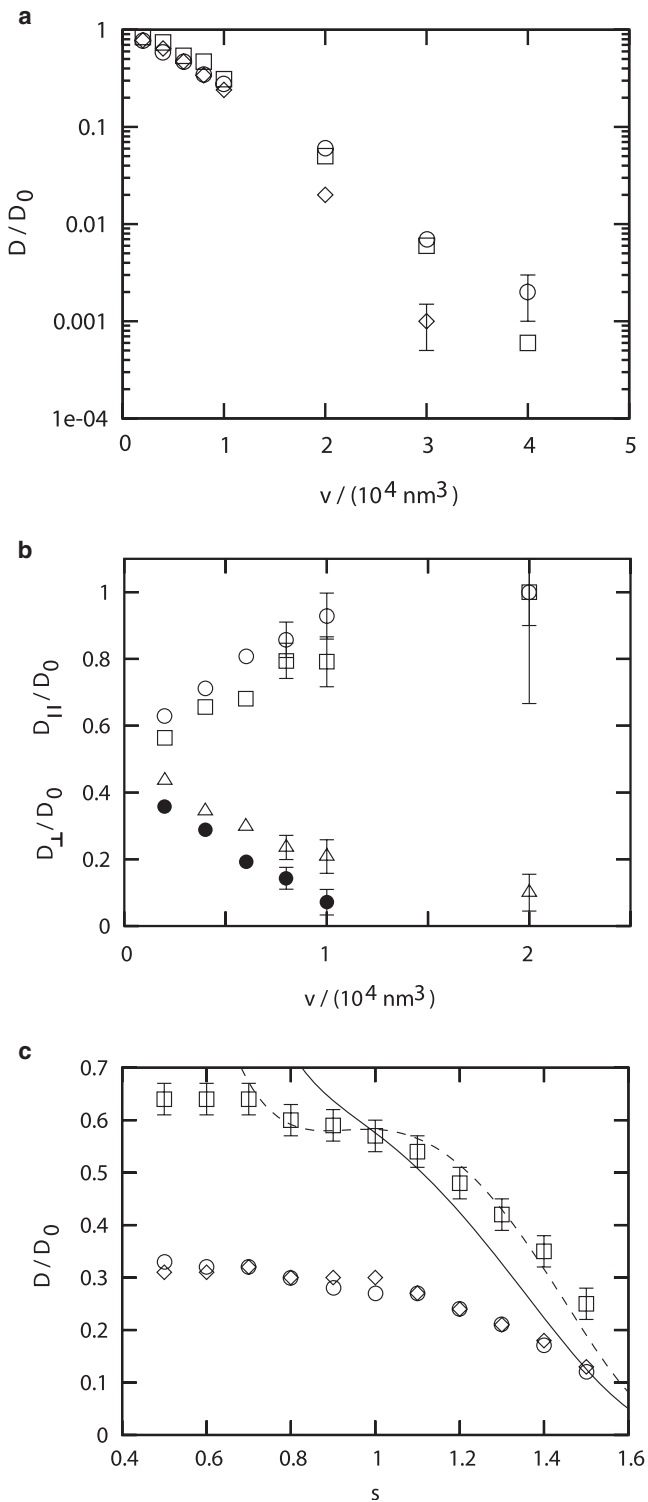$$\Gamma = \Gamma_0 \exp\left[-\frac{E_b}{k_B T}\right]. \tag{2}$$

FIGURE 6 RBC without ankyrin. (*a*) Ratio of reduced and free diffusion coefficient, D/D_0, for a protein that diffuses in the potential landscape of the cytoskeletal network that is unstretched (*squares*), stretched in *x* direction by a factor 1.5 (*circles*), and stretched in *y* direction by a factor 1.5 (*diamonds*), for several values of the interaction volume, *v* (see Fig. 3 for trajectories). The value of *D* is obtained from the mean-square displacement for long times. If no error bars are given, the error is smaller than the symbol size. (*b*) Relative contributions of the diffusion parallel and perpendicular to the

However, Arrhenian behavior is not expected for small barrier heights and for nontrivial barrier shapes, but is recovered for large barrier heights, i.e., for large values of *v*. In Fig. 6 *a*, the dependence of the diffusion coefficient on the effective interaction volume is similar to the temperature dependence that has been found for the random trap model for interstitial diffusion (69–71). In this model, the transition probability of a particle does not depend on the "direction", but only on the energy of the current position of the particle. Our potential landscape is more complicated than the idealized, pure barrier or pure trap models, and therefore requires the use of computer simulations instead of analytical theories to determine the effective diffusion coefficient.

In Fig. 6, *a* and *b*, the total and the directional diffusions parallel and perpendicular to the stretching are plotted for cytoskeletons that are anisotropically stretched with a factor 1.5 (and accordingly compressed in the perpendicular direction). For small values of the interaction volume, the influence of the cytoskeleton on the diffusion is small and the diffusion is almost isotropic. For large values of the interaction volume, the anisotropy increases until the diffusion takes place almost entirely parallel to the direction of the stretching. The orientation of the hexagonal network with respect to the direction of the stretching slightly influences the exact values of the predicted effective diffusion coefficients. In a real cell, the measured values of *D* will be averaged with respect to the orientation, due to the disordered nature of the RBC cytoskeleton (72).

Isotropic compression for $v = 6000$ nm^3 does not strongly affect the diffusion, whereas isotropic stretching reduces the effective diffusion coefficient (Fig. 6 *c*). In this figure we also plot an analytic expression that gives an estimate for the diffusion coefficient by assuming a simple one-dimensional hopping diffusion over barriers that are given by the value of the pressure difference at the midpoint between the anchors and in the center of the corral (for simplicity, we argue here for one dimension, but the argument also applies in two dimensions (73)).

Using Eq. 1,

$$D/D_0 \propto \exp\left[- v\left(p_{\mathrm{mid}} - p_{\mathrm{center}}\right)/k_{\mathrm{B}}T\right],$$

$$\text{where } p_{\mathrm{mid}} = \frac{4\left(d^2 + 2R_{\mathrm{g}}^2\right)}{\pi R_{\mathrm{g}}^2 d^3}, \tag{3}$$

the pressure in the middle of a bond, and p_{center} is the pressure in the center of a corral. For an unstretched cytoskeleton,

anisotropic stretch, $D_{\parallel}/D$ and $D_{\perp}/D$, for stretching in *x* (*open and solid circles*) and in *y* direction (*squares and triangles*). (*c*) Reduced diffusion for $v = 6000$ nm^3 and a cytoskeletal network that is isotropically compressed and stretched with the factor *s*: total diffusion D/D_0 (*squares*) and simple analytical models (*lines*, discussion in the main text) as well as contributions in *x* and in *y* direction, D_x/D_0 (*circles*) and D_y/D_0 (*diamonds*).
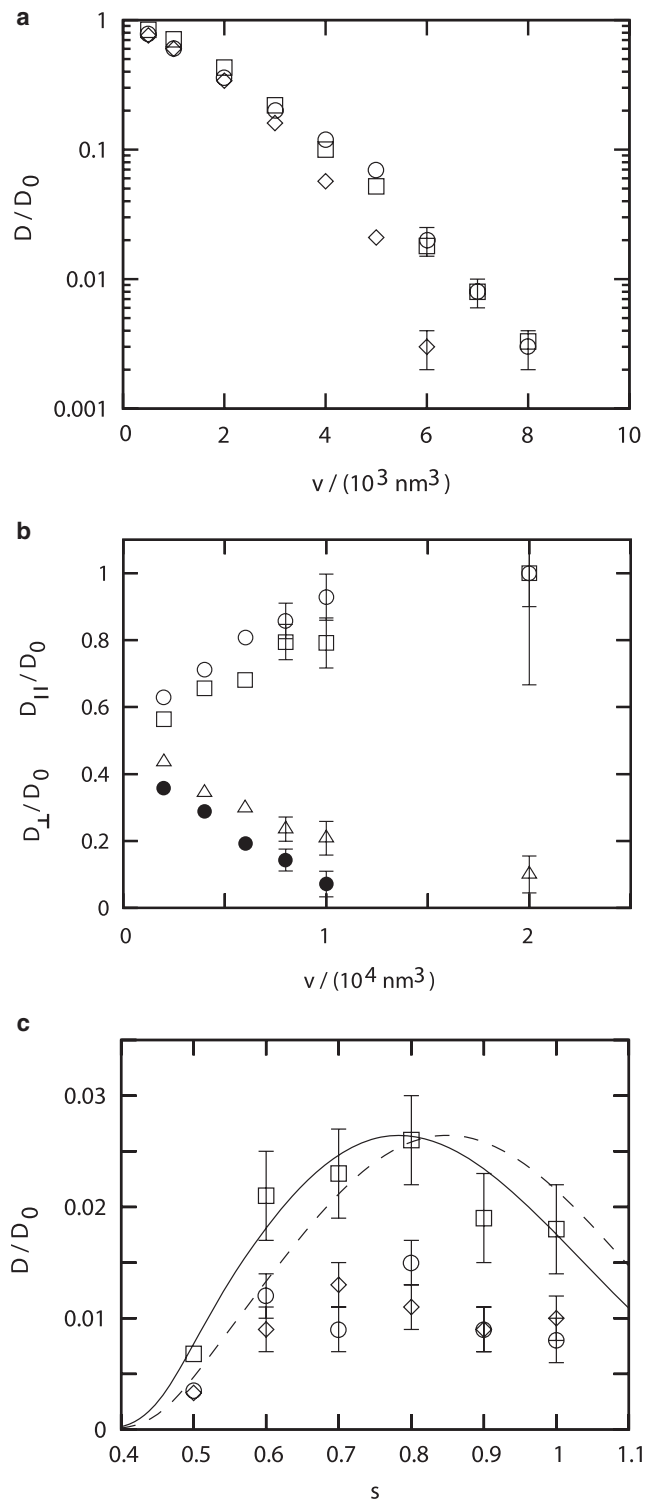
FIGURE 7 Same as Fig. 6, but for a RBC with ankyrin and thus in (*a* and *b*) for smaller values of the interaction volume. For isotropic stretching in (*c*), in the simulations the diffusion breaks down for $s > 1.0$.

$p_{center} \ll p_{mid}$; for small structure sizes, $s \lesssim 0.8$, we have to correct p_{mid} by adding up the pressure contributions from neighboring bonds. The corrected exponent reads

$-v(p_{mid} - p_{center} + 4\, p_{mid,nb})\, k_b T$, where $4\, p_{mid,nb}$ is the pressure at the midpoint due to the contributions of the neighboring bonds, and $p_{center} = 3\, p_{center,nb}$ is the pressure of the surrounding bonds in the center of the corral. (Contrary to the pressure at the midpoint of the bond by the bond itself, $p_{mid,nb}$ and $p_{center,nb}$ vanish exponentially with increasing distance from the anchor points.) Equation 3 should apply to the RBC whenever it applies to the simulations (Figs. 6 *c* and 7 *c*); in particular, Eq. 3 does not apply when the pressure fields of different cytoskeletal bonds overlap considerably. The overlap of the pressure fields is reduced by the additional ankyrin anchor, thus the expression holds up to smaller corral sizes for the RBC with ankyrin, compared with the RBC without ankyrin (compare Figs. 6 *c* and 7 *c*).

In Fig. 6 *c*, we rescale the function in Eq. 3, such that it best fits the simulations. The analytical model (*solid line*) therefore captures very well the functional form of the dependence of the diffusion on the distance between the anchors, *d*. An even better fit can be obtained if the size of the corral is taken into account by the prefactor *d/a* in front of the exponential function in Eq. 3 (*dashed line*) (35). For very small structure sizes, the pressure in the center of the corral exceeds the pressure at the midpoint of the bond, the potential landscape for the diffusion becomes more complicated and our analytical approximation is no longer appropriate.

RBC with ankyrin

Because of the close proximity of the cytoskeleton to the lipid bilayer, the effective diffusion coefficients in an intact RBC are considerably smaller than for the RBC without ankyrin (Figs. 6 and 7). To compare our calculations with experiments, we need to specify the effective interaction volume, *v*, for the protein of interest. The value of this parameter can be roughly estimated from the available structural data of the protein, as we show below. We can also extract this value by fitting the calculated reduction of the diffusion coefficient due to the cytoskeleton to the experimental data (8,52). We show that the estimated interaction volumes that we obtain using either method roughly agree.

The size of the cytoplasmic part of a protein can be estimated using available atomic force microscopy or electron microscopy images. For band 3, the cytoplasmic part has been characterized in Zhang et al. (74) and Wang et al. (75). and in the dimer state it consists of an elongated protrusion with volume $3.4 \times 7.5 \times 5.5\ \text{nm}^3 = 140\ \text{nm}^3$. The pressure field that the band 3 dimer interacts with is generated by the spectrin tetramer with diameter $\approx 5\ \text{nm}$ (76) and Kuhn length $\approx 5\ \text{nm}$. The overall excluded volume between the spectrin filament and the band 3 protein is therefore estimated to be $\approx 3600\ \text{nm}^3$. (For each side that the band 3 protein faces the cytoplasm, we have to add the spectrin diameter and the length that the spectrin molecule is stiff to estimate the total volume in which the protein affects the spectrin

conformations: $(3.4 + 10) \times (7.5 + 10) \times (5.5 + 10)$ nm$^3 \approx$ 3600 nm^3.) Note that the band 3 also forms tetramers of larger volumes (74), and has other proteins attached to its cytoplasmic domain, such as band 4.1, which further increase its effective volume in the cytoplasm.

We can calibrate v using experiments that measure the diffusion coefficients of proteins with and without cytoskeleton. In Sheetz et al. (8), 50 times faster diffusion of band 3 has been found in mouse erythrocytes that lack major components of the cytoskeleton ($D = 0.25$ μm^2 s^{-1}) compared with diffusion in the healthy cells ($D = 4.5$ 10^{-3} μm^2 s^{-1}). From Fig. 7 a, we find that a reduction of the effective diffusion coefficient by a factor of 1/50 corresponds to an interaction volume $v = 6000$ nm^3. Additionally, the ratio of the short-time to long-time diffusion coefficients observed for intact band 3 was found to be ≈ 100 (52), which corresponds to an interaction volume of $v \approx 6000$–7000 nm^3 in our calculations (Fig. 7 a). We therefore find that fitting the value of v to the observed diffusion coefficient, agrees with our previous estimate. Note that for the same interaction volume, our model predicts that the cytoskeleton in the ankyrin-deficient cells reduces the diffusion in the bilayer only by a factor of one-half for the unstretched cell (Fig. 6 a). The high sensitivity of the diffusion to the value of the interaction volume v, as shown in Figs. 6 and 7, means that the exact value of this parameter has to be extracted from diffusion experiments and is difficult to obtain from the molecular structure.

For trypsinized band 3, the ratio of the short-time to long-time diffusion coefficients was found to be ≈ 10 (52), which corresponds in our calculations to an interaction volume of $v \approx 3000$–4000 nm^3 (Fig. 7 a). Our model therefore predicts that the cytoplasmic interaction volume of band 3 is reduced by $\approx 50\%$ due to the trypsinization, which is a very substantial reduction of in the volume compared with the normal band 3. Note that even after trypsinization, the membrane domain of band 3 possesses a significant volume protruding into the cytoplasm (75), such that our estimate of a $\approx 50\%$ reduction is realistic. However, the estimate for the cleaved cytoplasmic volume that we calculated within our model is also an upper bound, because even for a membrane protein without any cytoplasmic domain, there is still the corralling effect due to the excluded volume of the anchor structures that are embedded within the bilayer ("picket-fence" model) (17,77). This is not explicitly included in our model. For an intact band 3 molecule, the picket fence of the anchor proteins is naturally taken into account, because at the locations of the anchors the cytoskeletal pressure is high and these picket regions are not accessible for the diffusing protein.

For a cytoskeleton that is stretched by a factor 1.5 and for $v = 6000$ nm^3, our model predicts a strongly asymmetric diffusion, which differs by about one order of magnitude between the parallel and perpendicular directions (Fig. 7 b). In the ankyrin-deficient case (Fig. 6 b), our model predicts a weaker asymmetry of the diffusion in such a stretched network.

In Fig. 7 c, isotropic compression for $v = 6\,000$ nm^3 hardly affects the diffusion, whereas isotropic stretching inhibits the proteins to leave the corral. We also plot the normalized analytical expression (for $s \lesssim 0.5$, the pressure at the midpoint is corrected by the pressure of the adjacent bonds), given in Eq. 3, which again shows very good agreement with the simulation results. The functional form is mainly determined by the value of the pressure at the midpoint (*solid line*), the geometric effect of the larger compartments has a minor influence (*dashed line*).

DISCUSSION

We propose what we believe is a new model for the steric hindrance of protein diffusion in the cell membrane that is directly related to the local density of flexible cytoskeletal filaments anchored to the membrane and to the protein size. We apply the model to calculate the effect of the spectrin cytoskeleton of RBC on the diffusion of the band 3 protein. The results presented in this study are for a hexagonal cytoskeletal network and are applied to the RBC, but the model applies whenever a cell has a cortical cytoskeleton of flexible polymers. (Steric hindrance has also been found for stiff, actin filaments that are parallel to the lipid bilayer (78). The appropriate model for this system is a rigid rod next to a fluctuating membrane (46).)

Our model goes beyond simple corral models, as it describes barrier heights and widths based on the physical properties of the cytoskeletal filaments. We are not only able to analyze experiments by assignment of barrier heights, but also to provide testable predictions. After determination of a protein-specific effective interaction volume, our model predicts the effect of a cortical cytoskeleton and of cytoskeletal changes on protein diffusion. In particular, we have studied the effect of stretching the cytoskeleton as well as the role of anchor complexes that connect the skeleton with the bilayer. From the good agreement between the expression given in Eq. 3 and the simulation results (Figs. 6 c and 7 c), we show that the hopping diffusion in such a system is dominated by the passages of the diffusing particle through the regions of lowest barrier height, which is at the midpoints between the anchored ends of the flexible protein (see typical trajectories in Fig. 3).

Experimentally, in membranes of RBCs that lack certain anchor proteins or components of the cytoskeleton, the diffusion coefficient increases with increasing deficit in cytoskeletal components (8,68); also cleavage of the cytoplasmic part of band 3 increases its diffusion (11,52). Similarly, an increase of the diffusion coefficient has been found if free spectrin anchor proteins have been added to perforated cells that compete with the attachment of the cytoskeleton to the bilayer. The increased diffusion coefficient by a factor 2 has been interpreted as being due to partial detachment of cytoskeleton and bilayer (79). Our calculations about the dramatic consequences of ankyrin anchors on the diffusion

in the RBC membrane can be useful in the study of hemo-lytic anemias where anchor complexes or linkages within the cytoskeleton are defective (80,81).

Deformation of a red blood cell in a micropipette leads to increased diffusion along the micropipette axis, which is the direction in which the cytoskeleton is strongly stretched (12,82). Both observations are in good agreement with our calculations (Figs. 6 and 7). Another experiment where hopping diffusion in a stretched membrane of the RBC has been observed is described in Tomishige et al. (52). Although this is the most direct experiment to date for the effects of stretching on the hopping diffusion, the short length of these trajectories (just as those shown in Fig. 3, *g* and *h*) make them inconclusive about the anisotropy of the long-time diffusion in the stretched network. Nevertheless, the local trajectories shown in Figs. 8 and 9 of Tomishige et al. (52) do indicate a somewhat preferred diffusion along the stretch direction, in agreement with our model's predictions. Quantitative evidence can be obtained from a long-time average over many trajectories in the stretched network, as shown in Figs. 6 *b* and 7 *b*. Such data awaits future experiments.

We note that additional processes, not included in our model, could result in enhanced diffusion perpendicular to the stretching direction. These processes are the breaking of the spectrin bonds, either by detachment from the anchor proteins (40) or by dimerization (60), and the unfolding of the individual spectrin molecules (61). The experimentally observed diffusion will result from the competition between the pressure field of the intact network and the processes mentioned above. If spectrin bonds preferably break while they are stretched (41), one could expect a higher diffusion in the direction perpendicular to the stretch. This is contrary to the predictions we calculate in this study for a fixed-connectivity network and serves as an example for how diffusion studies can be used as a tool to investigate the cytoskeleton properties (51,83). RBCs are stretched and deformed continuously in flow (84) as they pass through narrow capillaries (85). Whereas the bilayer can be observed directly during the cell deformation, much less is known about the cytoskeleton dynamics, although the cytoskeleton plays an important role for the elastic deformation properties (29) of the cell and its membrane fluctuations (86). Diffusion experiments in stretched cells may thus lead to a better understanding of the cytoskeleton (38,83).

Steric hindrance of the diffusion by the cytoskeleton is easy to explain for proteins, because proteins stick out of the lipid bilayer membrane. Interestingly, compartmentalized diffusion, hypothesized to be caused by the cytoskeleton, is also found for lipids that are observed on the outer leaflet of cellular membranes (while the cytoskeletal network is inside the cell) (17). This observation indicates that lipid diffusion may be indirectly influenced by the cytoskeleton via a picket fence model (17) or via coupling of the diffusion in the both layers of the membrane (87). (The picket fence model can be applied to protein diffusion with the fence being formed by the anchor proteins of the cytoskeleton. This is already included in our model; at the locations of the anchor proteins the polymer pressure is high such that the diffusing proteins have a low probability to be found there.)

Another example for an observation of anisotropic diffusion comes from the outer hair cell (88). In this cell, stretching the long axis of the cell gives rise to enhanced diffusion along the axis. Note that although this cell has a cytoskeletal network with different geometry, it also contains a spectrin network, somewhat similar to the RBC. We plan to address the specific geometry of these cells in our future studies.

Although the corral model is commonly hypothesized (and in case of the red blood cell, the cytoskeletal architecture strongly suggests a corral mechanism), it is not yet accepted for all cases for which it had been originally proposed (89,90). Other mechanisms, such as sticking, can also explain a reduced diffusion coefficient due to the presence of a cytoskeleton (23). Our calculation supports the hopping diffusion due to corralling in the case of the RBC membrane, in good agreement with Tomishige et al. (52). Furthermore, our calculation indicates that for small interaction volumes (or sparse anchoring) the hop diffusion does not manifest itself in a clear offset in the MSD plot for short times (Fig. 4, *inset*). Such a smooth crossover has also been observed experimentally in several systems (91).

We wish to stress that our model does not exclude other mechanisms that surely contribute to the observed diffusion of band-3 in the RBC membrane. Because we have a fit parameter in our model (the interaction volume *v*), we can use it to fit the data with our model alone, but we also show that the diffusion coefficient is very sensitive to small changes in this parameter (Figs. 6 *a* and 7 *a*). This means that the contribution due to other mechanisms can be accommodated easily because our structural estimate of the value of *v* is not precise enough. The use of a fit parameter in our model is not a disadvantage because any model requires some experimental, structural inputs. Other mechanisms that can be added to our model would need further experimental input or fit parameters. However, to avoid a large number of fit parameters, we analyzed the most simple case of a polymer network attached to a lipid bilayer first. Combining other effects to this basic model can now be done in a systematic manner, as the effects of each added mechanism can be studied.

The testable predictions of our model for the influences of stretching and of removal of anchor proteins on the diffusion might contribute to the verification of the corral mechanism. Measurements of the diffusion in the membrane can then be used as a tool to gain knowledge about cytoskeletal processes, such as active remodeling that depends on the ATP content of the cell (10,92). Anisotropic as well as isotropic stretching of the cortical cytoskeleton in cells might have a functional role by controlling diffusion.

REFERENCES

1. Lamb, T. D. 1996. Gain and kinetics of activation in the G-protein cascade of phototransduction. *Proc. Natl. Acad. Sci. USA*. 93:566–570.

2. McCloskey, M. A., and M. M. Poo. 1986. Rates of membrane-associated reactions—reduction of dimensionality revisited. *J. Cell Biol.* 102:88–96.

3. Dawes, A. T., and L. Edelstein-Keshet. 2007. Phosphoinositides and Rho proteins spatially regulate actin polymerization to initiate and maintain directed movement in a one-dimensional model of a motile cell. *Biophys. J.* 92:744–768.

4. Saxton, M. J. 1999. Lateral diffusion of lipids and proteins. *Curr. Top. Membr.* 48:229–282.

5. Henis, Y. I. 1993. Lateral and rotational diffusion in biological membranes. *In* Biomembranes: Physical Aspects. M. Shinitzky, editor, VCH, Weinheim. 279–339.

6. Saffman, P. G., and M. Delbruck. 1975. Brownian motion in biological membranes. *Proc. Natl. Acad. Sci. USA*. 72:3111–3113.

7. Gambin, Y., R. Lopez-Esparza, M. Reffay, E. Sierecki, N. S. Gov, et al. 2006. Lateral mobility of proteins in liquid membranes revisited. *Proc. Natl. Acad. Sci. USA*. 103:2098–2102.

8. Sheetz, M. P., M. Schindler, and D. E. Koppel. 1980. Lateral mobility of integral membrane proteins is increased in spherocytic erythrocytes. *Nature*. 285:510–512.

9. Sheetz, M. P. 1983. Membrane skeletal dynamics—role in modulation of red-cell deformability, mobility of transmembrane proteins, and shape. *Semin. Hematol.* 20:175–188.

10. Sheetz, M. P., and J. Casaly. 1980. 2,3-Diphosphoglycerate and ATP dissociate erythrocyte-membrane skeletons. *J. Biol. Chem.* 255:9955–9960.

11. Tsuji, A., and S. Ohnishi. 1986. Restriction of the lateral motion of band 3 in the erythrocyte membrane by the cytoskeletal network—dependence on spectrin association state. *Biochemistry*. 25:6133–6139.

12. Cho, M. R., D. W. Knowles, B. L. Smith, J. J. Moulds, P. Agre, et al. 1999. Membrane dynamics of the water transport protein aquaporin-1 in intact human red cells. *Biophys. J.* 76:1136–1144.

13. Koppel, D. E., M. P. Sheetz, and M. Schindler. 1981. Matrix control of protein diffusion in biological membranes. *Proc. Natl. Acad. Sci. USA*. 78:3576–3580.

14. Tank, D. W., E. S. Wu, and W. W. Webb. 1982. Enhanced molecular diffusibility in muscle membrane blebs—release of lateral constraints. *J. Cell Biol.* 92:207–212.

15. Murase, K., T. Fujiwara, Y. Umemura, K. Suzuki, R. Iino, et al. 2004. Ultrafine membrane compartments for molecular diffusion as revealed by single molecule techniques. *Biophys. J.* 86:4075–4093.

16. Marguet, D., P. F. Lenne, H. Rigneault, and H. T. He. 2006. Dynamics in the plasma membrane: how to combine fluidity and order. *EMBO J.* 25:3446–3457.

17. Kusumi, A., C. Nakada, K. Ritchie, K. Murase, K. Suzuki, et al. 2005. Paradigm shift of the plasma membrane concept from the two-dimensional continuum fluid to the partitioned fluid: high-speed single-molecule tracking of membrane molecules. *Annu. Rev. Biophys. Biomol. Struct.* 34:351–378.

18. Kusumi, A., Y. Sako, T. Fujiwara, and M. Tomishige. 1998. Application of laser tweezers to studies of the fences and tethers of the membrane skeleton that regulate the movements of plasma membrane proteins. *Methods Cell Biol.* 55:173–194.

19. Vaz, W. L. C., J. Stumpel, D. Hallmann, A. Gambacorta, and M. Derosa. 1987. Bounding fluid viscosity and translational diffusion in a fluid lipid bilayer. *Eur. Biophys. J.* 15:111–115.

20. Ollmann, M., A. Robitzki, G. Schwarzmann, and H. J. Galla. 1988. Minor effects of bulk viscosity on lipid translational diffusion measured by the excimer formation technique. *Eur. Biophys. J.* 16:109–112.

21. Boal, D. H., and S. K. Boey. 1995. Barrier-free paths of directed protein motion in the erythrocyte plasma membrane. *Biophys. J.* 69:372–379.

22. Forstner, M. B., D. S. Martin, F. Ruckerl, J. A. Kas, and C. Selle. 2008. Attractive membrane domains control lateral diffusion. *Phys. Rev. E Stat. Nonlin. Soft Matter Phys.* 77:051906.

23. Saxton, M. J. 2007. A biological interpretation of transient anomalous subdiffusion. I. Qualitative model. *Biophys. J.* 92:1178–1191.

24. Lillemeier, B. F., J. R. Pfeiffer, Z. Surviladze, B. S. Wilson, and M. M. Davis. 2006. Plasma membrane-associated proteins are clustered into islands attached to the cytoskeleton. *Proc. Natl. Acad. Sci. USA*. 103:18992–18997.

25. Johnson, S. J., T. M. Bayerl, W. H. Wo, H. Noack, J. Penfold, et al. 1991. Coupling of spectrin and polylysine to phospholipid monolayers studied by specular reflection of neutrons. *Biophys. J.* 60:1017–1025.

26. Bates, I. R., B. Hebert, Y. S. Luo, J. Liao, A. I. Bachir, et al. 2006. Membrane lateral diffusion and capture of CFTR within transient confinement zones. *Biophys. J.* 91:1046–1058.

27. Dertinger, T., I. von der Hocht, A. Benda, M. Hof, and J. Enderlein. 2006. Surface sticking and lateral diffusion of lipids in supported bilayers. *Langmuir*. 22:9339–9344.

28. Przybylo, M., J. Sykora, J. Humpolickova, A. Benda, A. Zan, et al. 2006. Lipid diffusion in giant unilamellar vesicles is more than 2 times faster than in supported phospholipid bilayers under identical conditions. *Langmuir*. 22:9096–9099.

29. Discher, D. E., N. Mohandas, and E. A. Evans. 1994. Molecular maps of red-cell deformation—hidden elasticity and in-situ connectivity. *Science*. 266:1032–1035.

30. Nigg, E. A., and R. J. Cherry. 1980. Anchorage of a band-3 population at the erythrocyte cytoplasmic membrane-surface—protein rotational diffusion measurements. *Proc. Natl. Acad. Sci. USA*. 77:4702–4706.

31. Corbett, J. D., P. Agre, J. Palek, and D. E. Golan. 1994. Differential control of band 3 lateral and rotational mobility in intact red blood cells. *J. Clin. Invest.* 94:683–688.

32. Gheber, L. A., and M. Edidin. 1999. A model for membrane patchiness: lateral diffusion in the presence of barriers and vesicle traffic. *Biophys. J.* 77:3163–3175.

33. Kusumi, A., H. Ike, C. Nakada, K. Murase, and T. Fujiwara. 2005. Single-molecule tracking of membrane molecules: plasma membrane compartmentalization and dynamic assembly of raft-philic signaling molecules. *Semin. Immunol.* 17:3–21.

34. Ritchie, K., X. Y. Shan, J. Kondo, K. Iwasawa, T. Fujiwara, et al. 2005. Detection of non-Brownian diffusion in the cell membrane in single molecule tracking. *Biophys. J.* 88:2266–2277.

35. Kenkre, V. M., L. Giuggioli, and Z. Kalay. 2008. Molecular motion in cell membranes: analytic study of fence-hindered random walks. *Phys. Rev. E Stat. Nonlin. Soft Matter Phys.* 77:051907.

36. Saxton, M. J. 1990. The membrane skeleton of erythrocytes—models of its effect on lateral diffusion. *Int. J. Biochem.* 22:801–809.

37. Saxton, M. J. 1989. The spectrin network as a barrier to lateral diffusion in erythrocytes—a percolation analysis. *Biophys. J.* 55:21–28.

38. Saxton, M. J. 1990. The membrane skeleton of erythrocytes—a percolation model. *Biophys. J.* 57:1167–1177.

39. Edidin, M., S. C. Kuo, and M. P. Sheetz. 1991. Lateral movements of membrane glycoproteins restricted by dynamic cytoplasmic barriers. *Science*. 254:1379–1382.

40. Gov, N. S., and S. A. Safran. 2005. Red blood cell membrane fluctuations and shape controlled by ATP-induced cytoskeletal defects. *Biophys. J.* 88:1859–1874.

41. Gov, N. S. 2007. Active elastic network: cytoskeleton of the red blood cell. *Phys. Rev. E Stat. Nonlin. Soft Matter Phys.* 75:011921.

42. Brown, F. L. H., D. M. Leitner, J. A. McCammon, and K. R. Wilson. 2000. Lateral diffusion of membrane proteins in the presence of static and dynamic corrals: suggestions for appropriate observables. *Biophys. J.* 78:2257–2269.

43. Leitner, D. M., F. L. H. Brown, and K. R. Wilson. 2000. Regulation of protein mobility in cell membranes: a dynamic corral model. *Biophys. J.* 78:125–135.

44. Lin, L. C. L., and F. L. H. Brown. 2005. Dynamic simulations of membranes with cytoskeletal interactions. *Phys. Rev. E Stat. Nonlin. Soft Matter Phys.* 72:011910.

45. Lin, L. C. L., and F. L. H. Brown. 2004. Dynamics of pinned membranes with application to protein diffusion on the surface of red blood cells. *Biophys. J.* 86:764–780.

46. Brown, F. L. H. 2003. Regulation of protein mobility via thermal membrane undulations. *Biophys. J.* 84:842–853.

47. Auth, T., S. A. Safran, and N. S. Gov. 2007. Filament networks attached to membranes: cytoskeletal pressure and local bilayer deformation. *New J. Phys.* 9:430.

48. Byers, T. J., and D. Branton. 1985. Visualization of the protein associations in the erythrocyte-membrane skeleton. *Proc. Natl. Acad. Sci. USA.* 82:6153–6157.

49. Lencesova, L., A. O'Neill, W. G. Resneck, R. J. Bloch, and M. P. Blaustein. 2004. Plasma membrane-cytoskeleton-endoplasmic reticulum complexes in neurons and astrocytes. *J. Biol. Chem.* 279:2885–2893.

50. De Matteis, M. A., and J. S. Morrow. 2000. Spectrin tethers and mesh in the biosynthetic pathway. *J. Cell Sci.* 113:2331–2343.

51. Tsuji, A., K. Kawasaki, S. Ohnishi, H. Merkle, and A. Kusumi. 1988. Regulation of band-3 mobilities in erythrocyte ghost membranes by protein association and cytoskeletal meshwork. *Biochemistry.* 27:7447–7452.

52. Tomishige, M., Y. Sako, and A. Kusumi. 1998. Regulation mechanism of the lateral diffusion of band 3 in erythrocyte membranes by the membrane skeleton. *J. Cell Biol.* 142:989–1000.

53. Tomishige, M., and A. Kusumi. 1999. Compartmentalization of the erythrocyte membrane by the membrane skeleton: intercompartmental hop diffusion of band 3. *Mol. Biol. Cell.* 10:2475–2479.

54. Reister-Gottfried, E., S. M. Leitenberger, and U. Seifert. 2007. Hybrid simulations of lateral diffusion in fluctuating membranes. *Phys. Rev. E Stat. Nonlin. Soft Matter Phys.* 75:011908.

55. Leitenberger, S. M., E. Reister-Gottfried, and U. Seifert. 2008. Curvature coupling dependence of membrane protein diffusion coefficient. *Langmuir.* 24:1254–1261.

56. Gov, N. S. 2006. Diffusion in curved fluid membranes. *Phys. Rev. E Stat. Nonlin. Soft Matter Phys.* 73:041918.

57. Saxton, M. J. 1995. Single-particle tracking—effects of corrals. *Biophys. J.* 69:389–398.

58. Bickel, T., C. Jeppesen, and C. M. Marques. 2001. Local entropic effects of polymers grafted to soft interfaces. *Eur. Phys. J. E.* 4:33–43.

59. Boal, D. H. 1998. Two-dimensional cytoskeletons under stress. *Biol. Bull.* 194:331–332.

60. An, X. L., M. C. Lecomte, J. A. Chasis, N. Mohandas, and W. Gratzer. 2002. Shear-response of the spectrin dimer-tetramer equilibrium in the red blood cell membrane. *J. Biol. Chem.* 277:31796–31800.

61. Johnson, C. P., H. Y. Tang, C. Carag, D. W. Speicher, and D. E. Discher. 2007. Forced unfolding of proteins within cells. *Science.* 317:663–666.

62. Kikuchi, K., M. Yoshida, T. Maekawa, and H. Watanabe. 1991. Metropolis Monte-Carlo method as a numerical technique to solve the Fokker-Planck equation. *Chem. Phys. Lett.* 185:335–338.

63. Auth, T., and G. Gompper. 2003. Self-avoiding linear and star polymers anchored to membranes. *Phys. Rev. E Stat. Nonlin. Soft Matter Phys.* 68:051801.

64. Winkler, R. G. 2003. Deformation of semiflexible chains. *J. Chem. Phys.* 118:2919–2928.

65. Winkler, R. G., and P. Reineker. 1992. Finite size distribution and partition functions of Gaussian chains—maximum-entropy approach. *Macromolecules.* 25:6891–6896.

66. Ursitti, J. A., D. W. Pumplin, J. B. Wade, and R. J. Bloch. 1991. Ultrastructure of the human erythrocyte cytoskeleton and its attachment to the membrane. *Cell Motil. Cytoskeleton.* 19:227–243.

67. Metropolis, N., and S. Ulam. 1949. The Monte Carlo method. *J. Am. Stat. Assoc.* 44:335–341.

68. Cho, M. R., S. W. Eber, S. C. Liu, S. E. Lux, and D. E. Golan. 1998. Regulation of band 3 rotational mobility by ankyrin in intact human red cells. *Biochemistry.* 37:17828–17835.

69. Mussawisade, K., T. Wichmann, and K. W. Kehr. 1997. Combination of random-barrier and random-trap models. *J. Phys. Cond. Mat.* 9:1181–1189.

70. Kehr, K., K. Mussawisade, and T. Wichmann. 1998. Diffusion of particles on lattices. *In* Diffusion in Condensed Matter. J. Kärger, P. Heitjans, and R. Haberlandt, editors. Vieweg, Braunschweig, pp. 265–305.

71. Mussawisade, K. 2000. Diffusion in models for disordered media without lattice-translational invariance. PhD thesis. Universität zu Köln.

72. Ursitti, J. A., and J. B. Wade. 1993. Ultrastructure and immunocytochemistry of the isolated human erythrocyte-membrane skeleton. *Cell Motil. Cytoskeleton.* 25:30–42.

73. Haus, J. W., K. W. Kehr, and J. W. Lyklema. 1982. Diffusion in a disordered medium. *Phys. Rev. B.* 25:2905–2907.

74. Zhang, D. C., A. Kiyatkin, J. T. Bolin, and P. S. Low. 2000. Crystallographic structure and functional interpretation of the cytoplasmic domain of erythrocyte membrane band 3. *Blood.* 96:2925–2933.

75. Wang, D. N., V. E. Sarabia, R. A. F. Reithmeier, and W. Kuhlbrandt. 1994. 3-Dimensional map of the dimeric membrane domain of the human erythrocyte anion exchanger, band 3. *EMBO J.* 13:3230–3235.

76. McGough, A. M., and R. Josephs. 1990. On the structure of erythrocyte spectrin in partially expanded membrane skeletons. *Proc. Natl. Acad. Sci. USA.* 87:5208–5212.

77. Bussell, S. J., D. L. Koch, and D. A. Hammer. 1995. Effect of hydrodynamic interactions on the diffusion of integral membrane proteins - diffusion in plasma membranes. *Biophys. J.* 68:1836–1849.

78. Morone, N., T. Fujiwara, K. Murase, R. S. Kasai, H. Ike, et al. 2006. Three-dimensional reconstruction of the membrane skeleton at the plasma membrane interface by electron tomography. *J. Cell Biol.* 174:851–862.

79. Fowler, V., and V. Bennett. 1978. Association of spectrin with its membrane attachment site restricts lateral mobility of human erythrocyte integral membrane proteins. *J. Supramol. Struct.* 8:215–221.

80. An, X. U., and N. Mohandas. 2008. Disorders of red cell membrane. *Br. J. Haematol.* 141:367–375.

81. Palek, J., and S. E. Lux. 1983. Red-cell membrane skeletal defects in hereditary and acquired hemolytic anemias. *Semin. Hematol.* 20:189–224.

82. Discher, D. E., and N. Mohandas. 1996. Kinematics of red cell aspiration by fluorescence-imaged microdeformation. *Biophys. J.* 71:1680–1694.

83. Saxton, M. J. 1992. Gaps in the erythrocyte-membrane skeleton—a stretched net model. *J. Theor. Biol.* 155:517–536.

84. Noguchi, H., and G. Gompper. 2005. Shape transitions of fluid vesicles and red blood cells in capillary flows. *Proc. Natl. Acad. Sci. USA.* 102:14159–14164.

85. Evans, E. A. 1989. Structure and deformation properties of red blood cells—concepts and quantitative methods. *Methods Enzymol.* 173:3–35.

86. Auth, T., S. A. Safran, and N. S. Gov. 2007. Fluctuations of coupled fluid and solid membranes with application to red blood cells. *Phys. Rev. E Stat. Nonlin. Soft Matter Phys.* 76:051910.

87. Merkel, R., E. Sackmann, and E. Evans. 1989. Molecular friction and epitactic coupling between monolayers in supported bilayers. *J. Phys.* 50:1535–1555.

88. de Monvel, J. B., W. E. Brownell, and M. Ulfendahl. 2006. Lateral diffusion anisotropy and membrane lipid/skeleton interaction in outer hair cells. *Biophys. J.* 91:364–381.

89. Daumas, F., N. Destainville, C. Millot, A. Lopez, D. Dean, et al. 2003. Confined diffusion without fences of a G-protein-coupled receptor as revealed by single particle tracking. *Biophys. J.* 84:356–366.

90. Wieser, S., M. Moertelmaier, E. Fuertbauer, H. Stockinger, and G. J. Schutz. 2007. (Un)confined diffusion of CD59 in the plasma membrane determined by high-resolution single molecule microscopy. *Biophys. J.* 92:3719–3728.

91. Suzuki, K., K. Ritchie, E. Kajikawa, T. Fujiwara, and A. Kusumi. 2005. Rapid hop diffusion of a G-protein-coupled receptor in the plasma membrane as revealed by single-molecule techniques. *Biophys. J.* 88:3659–3680.

92. Fowler, V., and D. Branton. 1977. Lateral mobility of human erythrocyte integral membrane proteins. *Nature.* 268:23–26.